PHILOSOPHICAL TRANSACTIONS A

Phil. Trans. R. Soc. A.
doi:10.1098/rsta.0223

Transformation of organic matter in a Barents Sea sediment profile: coupled geochemical and microbiological processes

Mark A. Stevenson[1], Johan C. Faust[2], Luiza L. Andrade[1], Felipe S. Freitas[3], Neil D. Gray[1], Karen Tait[4], Katharine R. Hendry[3], Robert G. Hilton[5], Sian F. Henley[6], Allyson Tessin[7], Peter Leary[1], Sonia Papadaki[3], Ailbe Ford[2], Christian März[2], Geoffrey D. Abbott[1]

[1]School of Natural and Environmental Sciences, Newcastle University, Newcastle upon Tyne, NE1 7RU, UK
[2]School of Earth and Environment, University of Leeds, Leeds, LS2 9JT, UK
[3]School of Earth Sciences, University of Bristol, Bristol, BS8 1RJ, UK
[4]Plymouth Marine Laboratory, Prospect Place, Plymouth PL1 3DH, UK
[5]Durham University, Geography, Science Laboratories, South Road, Durham, DH1 3LE, UK
[6]School of GeoSciences, University of Edinburgh, James Hutton Road, Edinburgh EH9 3FE, UK
[7]Department of Geology, Kent State University, Kent, OH, 44240, USA

Mark Stevenson DOI: 0000-0002-8955-0855
Geoffrey D. Abbott DOI: 0000-0001-9803-8215
Neil Gray DOI: 0000-0002-2395-4320
Katharine R. Hendry DOI 0000-0002-0790-5895
Felipe S. Freitas DOI: 0000-0001-8279-5772

Keywords: Barents Sea, carbon cycling, microbial processes, geochemistry, marine sediment, organic matter reactivity.

Summary

Process-based, mechanistic investigations of organic matter transformation and diagenesis directly beneath the sediment-water interface in Arctic continental shelves are vital as these regions are at greatest risk of future change. This is in part due to disruptions in benthic-pelagic coupling associated with ocean current change and sea ice retreat. Here we focus on a high-resolution, multi-disciplinary set of measurements that illustrate how microbial processes involved in the degradation of organic matter are directly coupled with inorganic and organic geochemical sediment properties (measured and modeled) as well as the extent/depth of bioturbation. We find direct links between aerobic processes, reactive organic carbon and highest abundances of bacteria and archaea in the uppermost layer (0-4.5 cm depth) followed by dominance of microbes involved in nitrate/nitrite and

*Author for correspondence (mark.stevenson@newcastle.ac.uk).
†Present address: School of Natural and Environmental Sciences Newcastle University, Newcastle upon Tyne, NE1 7RU, UK

iron/manganese reduction across the oxic-anoxic redox boundary (~4.5-10.5 cm depth). Sulfate reducers dominate in the deeper (~10.5-33 cm) anoxic sediments which is consistent with the modeled reactive transport framework. Importantly, organic matter reactivity as tracked by organic geochemical parameters (*n*-alkanes, *n*-alkanoic acids, *n*-alkanols and sterols) changes most dramatically at and directly below the sediment-water interface together with sedimentology and biological activity but remained relatively unchanged across deeper changes in sedimentology.

Main Text

Introduction

Organic matter (OM) processing and transformation at the seafloor, ultimately drives the sequestration of organic carbon and the biogeochemical modifications that occur prior to long-term burial [1]. Across this important marine transition zone biological, geological and physical processes take place at variable rates, including deposition of organic and inorganic material, partial degradation of OM by microbes, sediment mixing by benthic fauna and, dissolution and precipitation of mineral phases. Interactions between these coupled processes are typically poorly characterised, but it is increasingly recognised that it is the combined biogeochemical properties of sediments adjacent to OM that determine its degradation and preservation trajectories [1], with alterations to the fate of deposited OM particularly prevalent in high-latitude oceans. Arctic seafloor sediments are, sensitive to changes in pelagic to benthic coupling as a result of alterations in the distribution of water masses and sea-ice extent linked to climate changes [2], with process-based coupled sedimentary organic-inorganic-microbial studies useful to capture the detail in the key diagenetic processes and interactions which occur during OM transformation. It is also important to distinguish external parameter changes that have impacts on organic carbon reactivity from those that do not.

The OM at and below the Arctic shelf seafloor sustains a key ecological niche, including high microbial diversity [3] and a rich benthic ecosystem [4]. Processing of organic carbon at the seafloor is closely linked to water column productivity [5] and to delivery of algal biomass from melting sea ice [6]. Over longer timescales marine organic carbon burial is the principal mechanism of millennial scale carbon sequestration [7, 8] which, subject to processing and transformation, becomes part of the geological record [9].

OM deposited at the seafloor undergoes intensive diagenetic transformation, with up to ~99% degraded at the sediment-water interface (SWI), escaping long-term burial [10]. At the SWI, the extent of transformation of OM results from the complex interactions between OM composition and its stability to processing (e.g. redox conditions, microbial community structure, mineralogy) [11, 12]. Consequently, such interactions result in distinct OM reactivity changes during burial and differences in the rates of early diagenesis between autochthonous (typically more reactive) and allochthonous sources (typically less reactive) [13]. OM which 'survives' the uppermost sediment layer is subject to further microbial activity where polymer hydrolysis, iron and manganese reduction, denitrification, nitrate dissimilation, sulfate reduction and methanogenesis take place. Microbes indicative of these processes inhabit often clearly stratified communities [14-16]. As OM is gradually broken down, only the least reactive OM is left behind [17]. Redox processes, whereby sediments transition from oxic to anoxic conditions, are an additional control on OM reactivity as anaerobes inhabiting oxygen-free environments are limited in their ability to hydrolyze more structurally complex compounds [10]. Simultaneously, bioturbating animals which burrow into and physically mix sediments help control the thickness of the oxic layer, regulating the amount and quality of organic carbon accumulated [18].

We selected the Barents Sea seafloor as our study location because it is characterised by a mix of marine and terrestrial organic matter input, a clearly defined sequence of microbially controlled redox zones, a variable input of inorganic material from land, and a strong seasonality that affects chemical, physical and biological processes in a predictable manner. The Barents Sea is also known to be vulnerable to climate change, with the existing extent of sea ice loss expected to intensify in Arctic regions over the coming decades [19-21]. As well as having a clear impact on wider Earth system processes [22, 23], sea ice loss driven by atmospheric and oceanic warming is modifying the timing and abundance of biological productivity within the Barents Sea by altering water column stratification [24], including the relative balance of Arctic and Atlantic water masses [25], potentially altering the type of OM delivered to the seafloor.

Although previous studies have combined microbiological and geochemical measurements in Arctic continental shelf settings, they tend to focus on surface sediment transects [26], down-core at low-resolution in deeper sediments [15, 16, 27, 28], or were limited by sequencing libraries and study location [14], and so unable to show so clearly the depth-

successional redox transition close to the SWI. By using these techniques in tandem, it is possible to fully explore the microbiological and geochemical basis underpinning diagenetic models [29] highlighting the complexity of these processes and enabling quantification.

The main objective of this study is to improve our understanding of the interactions that regulate and mediate OM processing at and below the SWI, by combining downcore organic, inorganic and microbial measurements from the north western Barents Sea. We aim to link biological and mineralogical mediated geochemical changes, by providing insight into the reactivity of OM as a function of down-core trends in the context of microbial abundances and activities related to redox processes. Overall, we expected that the uppermost sediments would show evidence of a rapid decrease in the reactivity of OM associated with the oxic layer, aerobic microbial activity, and biological sediment mixing (the bioturbated layer). Beneath, we used our set of multi-disciplinary measurements to assess the extent to which highly reactive carbon inputs are mineralised before cessation of aerobic processes, and whether reactive carbon survives the transition to anoxia. We include inorganic geochemical and grain size measurements to assess how changes in sedimentation over the later Holocene affect trends in organic geochemical parameters.

Methods

i) Study sites and sampling

Two sediment cores from the same location (B15) were obtained during the JR16006 cruise (2017) of the RRS James Clark Ross in the Barents Sea [30] and included multicore sampling from station B15 E144 (78.25169 °N; 30.00909 °E) for depth resolved organic geochemistry [31], microbial abundances and community compositions, and B15 E146 (78.25152 °N; 30.00849 °E) for inorganic geochemistry, to 33 cm depth (Supplements: Table S1). Station B15 is located to the east of Svalbard's Edge Island and south of the island of Kongsoya (Supplements: SI Fig. 1) and was sea-ice-covered during sampling [32]. The sediments were taken from 315 m water depth in a glacial trough. Cores were sectioned at 0.5 cm intervals to 2 cm depth and at 1 cm intervals to the base of the core. Sections were stored and flash frozen in combusted foil (organic geochemistry (flash frozen −80 °C, stored −20 °C)), plastic bags (inorganic geochemistry (−20 °C)), and plastic vials (microbiology (−80 °C)).

ii) Bulk organic geochemistry

Total organic carbon (TOC) was analysed on freeze-dried acidified sediments (HCl; 4M; 4 h), dried overnight (60 °C) and analysed with a CS230 Carbon/Sulfur Determinator (Leco Corporation, Michigan, USA) using porous crucibles. The TOC content is expressed as the weight percentage of dried sediment (wt.%). Nitrogen measurements were made using a Vario MAX CNS analyser (Elementar, Langenselbold, Germany). TOC:N ratios were not corrected for the molar weight of C and N. Stable nitrogen isotope measurements ($\delta^{15}N$) were performed using an ECS 4010 Elemental Analyser (Costech Analytical Technologies Inc., Valencia, CA) coupled to a Delta V Advantage (Thermo Finnigan, Hemel Hempsted, UK) isotope ratio mass spectrometer and are reported in (δ) notation in per mille (‰) relative to atmospheric N_2 (AIR). Sample precision was <0.2‰.

iii) Grain size analysis

Bulk sediment samples were disaggregated in an ultrasonic bath (15 minutes) and analysed on a Mastersizer 2000E laser diffractometer for particles of a diameter range 0.1-1000 μm at the University of Leeds. Results were categorised into 6 size fractions and are presented as cumulative volume percentages.

iv) Molecular organic geochemistry

Lipids were extracted and analysed in a similar method to Holtvoeth *et al.* [33]. Briefly, freeze-dried sediment (3-4 g) spiked with internal extraction standard (5α-androstane) was sonicated in dichloromethane: methanol (9:1 v/v) three times (15 mins each), with the resulting total lipid extract (TLE) concentrated, left overnight in the presence of activated copper to remove sulfur and passed through an anhydrous sodium sulfate column to remove water. Transmethylation was performed by adding acetyl chloride in methanol (1:30 v/v) at 45 °C, left overnight and followed by a clean-up step with potassium carbonate to neutralise excess acids. Prior to analysis, derivatisation of compounds containing hydroxyl groups was performed using N,O-bis(trimethylsilyl)trifluoroacetamide (BSTFA) with 1% trimethylchlorosilane (TMS) at 65 °C for 1 h.

Samples were injected (1 μl) into an Agilent 7890B Gas Chromatograph (GC) coupled to a 5977B MSD Mass Spectrometer (MS) operated in full scan mode (70 eV; source temp 230 °C;

helium flow rate 1 mL/min). A 60 m J&W Scientific HP-1ms fused silica capillary column was used for GC separation (0.25 mm x 0.25 µm) with an oven temperature of 6 °C/min to 170 °C; hold of 1 min; followed by a slower ramp of 2.5 °C/min to 315 °C and a hold of 22 min. Compounds were identified from their respective mass spectra and retention times, with quantities calculated relative to the peak area of the internal standard 5α-androstane and an assumption of a 1:1 response.

For *n*-alkanoic acids parameters include total FAMEs (fatty acid methyl esters), ratio of the C_{15} anteiso/C_{16} FAME, terrigenous to aquatic fatty acid ratio (TAR_{FA}) [34] and total carbon preference index (CPI_T) [35]. For sterols parameters include cholesterol/brassicasaterol, cholesterol/β-sitosterol, stigmasterol/stigmastanol and β-sitosterol/stigmastanol. For *n*-alkanes parameters were carbon preference index (CPI) [36] and odd over even predominance for *n*-$C_{17\text{-}21}$ & *n*-$C_{21\text{-}25}$ ($OEP_{17\text{-}21\ \&\ 21\text{-}25}$) [37]. Terrestrial to aquatic ratio (TAR) and Aut/All (autochthonous/allochthonous) ratio was selected for *n*-alkanols [38]. Error displayed is the standard deviation of a sample analysed in triplicate.

v) Inorganic geochemistry

X-ray fluorescence (XRF) was performed on freeze dried and gently grinded sediment samples (700 mg) from B15 E146, mixed with di-lithiumtetraborate (4200 mg, $Li_2B_4O_7$, Spectromelt A10), preoxidized at 500 °C with 1.0 g NH_4NO_3 (p.a.) and fused to homogenous glass beads. Samples were analysed using a PW-2400 WD-XRF Scanner (Philips, Netherlands) calibrated with geostandards at the University of Oldenburg with Fe, P and Mn used in this study. Analytical precision and accuracy was <5%.

vi) Microbiology

Genomic DNA was extracted using the DNeasy® PowerSoil® kit (QIAGEN, Hilden, Germany). Concentration and viability were tested using Qubit™ (Thermo Fisher Scientific, Waltham, Massachusetts, USA) and polymerase chain reaction (PCR) respectively, prior to sequencing. High throughput DNA sequencing was performed by the NUomics sequencing service at Northumbria University (UK). 16S rRNA gene libraries were prepared following protocol [39], in which each fragment was composed by an Illumina adapter, followed by an index sequence (only for forward primer), a 10-nt pad to avoid formation of hairpin structures, linkers and the V4 region specific either forward or the reverse primer. Primers

used were 4515F (GTGYCAGCMGCCGCGGTAA) and 806R (GGACTACHVGGGTWTCTAAT) as per the Earth Microbiome Project protocol [40]. Sequencing was performed on the MiSeq Personal Sequencer (Illumina, San Diego, CA, USA) using the V2 500 reagent kit. Demultiplexed paired end FASTQ files were analysed using QIIME2 [41] using a pipeline (https://github.com/peterleary/markergene). Amplicon sequence variants were generated in QIIME2 using DADA2 [42] and taxonomy was classified using the SILVA 132 reference database [43]. Taxonomic abundance data is expressed as percentage abundance (%) enumerated from fractional abundances in sample libraries.

Quantitative PCR (qPCR) was used to determine the abundance of archaeal and bacterial 16S rRNA genes using the following primer pairs: Parch519F (CAGCCGCCGCGGTAA) and ARC915R (GTGCTCCCCCGCCAATTCCT) [44] for archaea and Bact1369F (CGGTGAATACGTTCY-CGG) and Prok1492R (GGWTACCTTGTTACGACTT) [45] for bacteria using primer concentrations and qPCR cycling conditions described in [46] and a LightCycler 96 instrument (Roche Life Science, Penzberg, Germany). Assays contained a standard curve ranging from 10^2 to 10^8 amplicons μl^{-1} using cloned sequences. rRNA numbers were quantified via comparison to standard curves using the Lightcycler 96 detection software. No-template controls were below the threshold in all experiments. Measurements of 16S rRNA for bacteria and archaea are presented as copies of genes per gram/wet weight sediment.

vii) Complementary measurements and datasets

To provide constraint on the long-term sedimentation rates at the study site (and provide a temporal framework to interpret the results) radiocarbon measurements (^{14}C-AMS) were carried out on mixed foraminifera picked from samples at 27.5 cm depth, near the base of the core. Sediment was dried, disaggregated, filtered and sieved (>125 μm). Light microscopy was used to pick and sort benthic and planktonic foraminifera tests for the Mini Carbonate Dating System (MICADAS) (Ionplus, Dietikon, Switzerland) at the University of Bristol. Measurements of ^{14}C were performed on both samples without graphitisation, but with an acidification step, followed by analysis in the presence of a gas-ion source [47]. Bayesian calibration was carried out in MATLAB [48]. Acknowledging the challenges that would be encountered by developing a sediment mass accumulation rate (MAR) on the basis of a single point and its likely difference compared with a recent radionucleotide

approach [49], instead here we calculate percentage yr^{-1} TOC loss based on the youngest basal age to provide an estimation and comparison of reactivity between oxic and anoic parts of the core.

We sourced empirical data on macrofaunal particle reworking from Solan *et al.* [50] based on sediment profile imaging of introduced optically distinct particle tracers (luminophores) to the surface of sediment cores after 12 days incubation [51]. Specifically, values for the mean mixed depth ($^{f\text{-}SPI}L_{mean}$, time dependent indication of short term faunal mixing, [52]) and the maximum mixed depth ($^{f\text{-}SPI}L_{max}$, maximum vertical extent of faunal mixing [52]) are presented alongside organic geochemical (Fig. 2) and microbial parameters (Fig. 3).

Porewater analysis of oxygen (O_2) was completed on sediment cores from the same station (B15) in 2019 using a portable O_2 probe, with data sourced from Freitas *et al.* [29] and presented against changes in microbial parameters (Fig. 3).

Modeled estimations of the relative contribution of metabolic pathways (aerobic respiration (O_2 – M), denitrification (NO_3 – M), iron reduction ($Fe(OH)_3$ – M), sulfate reduction (SO_4 – M) and manganese reduction (MnO_2 – M) to based on reactive transport modelling are from Freitas *et al.* [29] and are also presented against changes in microbial parameters (Fig. 3). We additionally include model-derived oxygen concentration depth profiles (SI Fig. 2 & 3) [29].

viii) Statistical analysis

Data was explored for correlations between bulk variables, organic geochemistry, geomicrobiology, porewater oxygen and modeled metabolic pathway processes, with statistically significant relationships (using Pearson's correlation) listed in Fig. S2-S6. Modeled datasets were resampled in Matlab (ver. R2019a) to the same depth intervals using spline interpolation. Principal components analysis (PCA) was conducted due to short DCA gradient lengths (<2) in Canoco v4.51 [53] on log_{10} transformed and centred data, with samples highlighted in blue for proximity to the maximal extent of faunal reworking (Fig. 4). Microbial taxa (defined by presence, absence and abundance), geochemical concentrations and modeled percentage contribution of metabolic pathways to OM heterotrophic degradation were included in the PCA table to create dissimilarity distances and eigenvalues of the samples, with the two largest PCs plotted and superimposed over samples.

Results

An age-estimation was carried out at 27.5 cm depth with a mixed planktonic foraminifera ^{14}C-AMS age of 4075 ± 180 (1σ) ^{14}C year, calibrated to a median age of 4121 cal. yr BP (3632 to 4612 cal. yr BP, 95% confidence interval, Fig. 1). At the same depth, a paired mixed benthic foraminifera measurement gave a ^{14}C-AMS age of 5079 ± 91 (1σ) ^{14}C, calibrated to a median age of 5433 cal. yr BP (5245 to 5630 cal. yr BP, 95% confidence interval). Differences in the shape of planktonic compared with benthic foraminifera make them susceptible to bioturbation and sedimentation at different rates, providing ^{14}C evidence of key processes taking place in this system.

TOC content declined from a maximum of 1.78 wt.% at ~2.5 cm to minima of 1.33 wt.% at ~10.5 cm and 1.28 wt.% at ~32.5 cm (Fig. 1). Total N followed a similar trend, declining rapidly from 0.23 wt.% at the top of the core to 0.17 wt.% by ~10.5 cm and 0.15 wt.% at the base (Fig. 1). The ratio of TOC:N fluctuated throughout the core but gradually increased as a function of burial depth trend from a minimum of 7.5 at the top of the core to a maximum of 9.2 close to the base. The nitrogen isotope ratio (δ^{15}N) declined from a maximum of 7.1‰ at the top of the core to a minimum of 5.8‰ at the base.

Profiles of total Fe and P concentrations displayed similar trends but with different magnitudes and were stable (5.1-5.6% and 0.16-0.17%, respectively) from the SWI to ~9.5 cm, below this depth, Fe and P increases to a maximum of 8.4% Fe and 0.3% P at a clear peak by ~14.5 cm. Below this peak Fe and P sharply declined to minimum values by ~16.5 cm with Fe ranging from 4.3% to 5.0% and P ranging from 0.11% to 0.13% to the bottom of the core. Total Mn was highest in the upper part of the core, peaking at ~4.5 cm at 1.02% and again at 8.5 cm to 0.96%, followed by a decline to low concentrations by ~10.5 cm which remained low to the base of the core.

Grain size was dominated by clay and silt from the top of the core (cumulative <63 μm fraction ~78%) to ~0.75 cm where coarser particles >63 μm (mainly fine sands) accounted for ~82% of the fraction until ~2.5 cm where finer particulates again dominated (<63 μm fraction >89%) (Fig. 1). Finer silts then decreased to < 16% (<63 μm fraction) by 5.5 cm, with a marked increase at ~14.5 cm to ~53 % coincident with Fe and P peaks. By ~19.5 cm finer

silts returned to previous levels <16% (<63 μm fraction), before a gradual rise from ~24 cm, peaking at ~90% from ~30.5 cm to the base of the core.

Organic geochemical ratios of key compounds displayed clear changes in the uppermost ~9.5 cm of the core, with the most pronounced changes coincident with maximum bioturbation in the top ~4.5 cm (4.3 cm is greatest of three maximum bioturbation replicates [50]) (Fig. 2). Some compounds had especially pronounced changes in the uppermost sample coincident with mean bioturbation at 0.5 cm (0.5 cm is the average of three mean bioturbation replicates [50]). Total FAMEs declined rapidly from >1400 $\mu g\ g^{-1}$ TOC at 0.5 cm to ~ 200 $\mu g\ g^{-1}$ TOC at ~2 cm, with subsequent values ranging narrowly between ~200 and 500 $\mu g\ g^{-1}$ TOC to the base (Fig. 2). The ratio of C_{15} anteiso:C_{16} FAME, an indicator of microbial activity, was high in samples just below the sediment surface, within maximum bioturbation (0-4.3 cm) from ~0.75-2.5 cm with values 0.15-0.19 and also at ~5.5 cm with a value of 0.18, followed by a general declining trend to ~25.5 cm (0.06). TAR_{FA} increased from a minimum of ~0.1 at the top of the core to a maximum of ~1.2 at ~1.75 cm within the zone of maximum bioturbation. The CPI_T ratio for *n*-alkanoic acids was high in the uppermost sample (~13.5) coincident with mean bioturbation, declining to fluctuations between ~5 and 9.4 to the base.

The ratio of cholesterol/brassicasterol was low at the top of the core (<1.3), increasing to ~3 (2.5 cm) within the zone of bioturbation, before decreasing to <1.8 by ~3.5 cm, with a further peak to ~2.4 at ~9.5 cm. Similarly, cholesterol/ β-sitosterol also peaked at ~2.5 cm depth (to >4), prior to a general decrease to the base of the core (<1.3). In contrast, stigmasterol/stigmastanol declined from a maximum of 1.0 at the top of the core to 0.2 at ~9.5 cm, followed by fluctuations between 0.1 and 0.4 to the base. Similarly, the ratio of sterols β-sitosterol/stigmastanol declined rapidly from a peak of 4.2 at the top of the core to ~1.2 by ~9.5 cm, remaining stable to the base of the core (1.4 to 0.9). The CPI ratio for *n*-alkanes declined from a maximum of 2.5 at the top of the core to 1.7 at a depth of ~9.5 cm below the seafloor. With further increase in burial depth to ~17.5 cm, there was a subsequent smaller increase in CPI with values for deeper horizons below this ranging from 1.9 to 1.7. The OEP for *n*-alkanes from C_{21}-C_{25} ranged from a maximum of 1.6 at the top of the core to a minimum of 1.1 by ~3.5 cm, with values below this fluctuating between 1.1 and 1.2. OEP for *n*-alkanes $C_{21\text{-}25}$ were especially prominent in the uppermost sample (~1.6) coincident with mean bioturbation, with all values below this <1.3. The TAR index for *n*-alkanes increased from a maximum of ~1 at the top of the core to >4 at ~9.5 cm, prior to

fluctuations between ~2 and ~3.3 to the base. The autochthonous/allochthonous ratio for *n*-alkanols also showed a decline in the uppermost layer from a maximum of 0.9 at the top of the core to a minimum of 0.4 by ~9.5 cm.

16S rRNA gene counts representative of bacterial and archaeal cell numbers fluctuated but were present in abundance from the SWI down to ~11.5 cm, below which abundances were orders of magnitude lower (Fig. 3). For bacterial 16S rRNA genes above 11.5 cm the mean was 3.32×10^7 copies g^{-1} wet sediment, declining markedly to 9.23×10^5 copies g^{-1} wet sediment below 11.5 cm, while for archaea the mean above 11.5 cm was 7.28×10^7 copies g^{-1} wet sediment declining to 2.31×10^6 copies g^{-1} wet sediment (Fig. 3). The greatest peaks in bacterial and archaeal 16S rRNA genes were within the uppermost ~4.5 cm coincident with most intense bioturbation. The progressive decline in these numbers could either be attributable to the balance between depositional inputs at the surface and subsequent death and cell lysis with sedimentation, or may relate to in-situ growth. Based on 16S rRNA gene sequence analysis these depth related declines in absolute abundances were accompanied by distinctive successional changes in the relative abundances of some dominant archaeal and bacterial taxa indicative of a depth related transition from aerobic to anaerobic microbial processes, linked to bioturbation depth. For instance, 16S rRNA gene sequences related to the BD7-8 marine group [54] declined sharply from a maximum of 2.36% of sequences in the amplicon library at the top of the core to 0% by ~5.5 cm, with only minor occurrences in amplicon libraries from depths below this (Fig. 3). Group BD7-8 is considered cosmopolitan in marine benthic habitats and are putative aerobic and nitrate reducing mixotrophs [55, 56]. Declines in group BD7-8 were coincident with both decreases in measured ($R=0.97$, $p < 0.01$) and modeled ($R = 0.94$, $p < 0.01$) O_2 concentration depth-profiles (Supplements; Figure S2) and the zone of bioturbation (Fig. 3). Highlighting links between organic matter quality and aerobic processes, there were positive correlations between CPI for *n*-alkanes and both measured ($R = 0.81$, $p < 0.05$) and modeled ($R= 0.92$, $p < 0.01$) O_2 concentration depth-profiles (Supplements, Figure S2). Similar positive correlations between modeled relative oxygen contribution, $\delta^{15}N$ ($R = 0.89$, $p < 0.01$), %N ($R = 0.93$, $p < 0.01$) and %TOC ($R = 0.86$, $p < 0.01$) were found, with similar but slightly weaker correlations between model-derived O_2 concentration depth-profiles and $\delta^{15}N$ ($R = 0.83$, $p < 0.01$), %N ($R = 0.88$, $p < 0.01$) and %TOC ($R = 0.84$, $p < 0.01$) (Supplements; Figure S3). Corroborative of the presence and depth related consumption of molecular oxygen in the upper few cm (above ~9.5 cm) of the sediment, sequences related to aerobic ammonia

oxidizers from the family *Nitrosopumilaceae* [57] followed a general declining trend from the top of the core to the base, although their abundance varied (Fig. 3). *Nitrosopumilaceae* was negatively correlated with TOC:N ratio ($R = 0.62$, $P < 0.01$) and positively correlated with $\delta^{15}N$ ($R = 0.91$, $p < 0.01$) (Supplements; Figure S4).

In contrast to these depth related declines, sequences related to the putatively iron reducing *Shewanellaceae* family [58] which variably increased their abundance in amplicon libraries were persistent up to ~10.5 cm (Fig. 3). Similarly, sequences related to the *Desulfuromondales* family (also putatively capable of iron reduction [59]) generally increased their relative abundances up to ~10.5 cm but with an additional peak at ~15.5 cm. Likewise, sequences related to the family *Methylomirabilaceae* (capable of methane oxidation coupled to nitrite reduction [60]) increased in abundance at the top of the core peaking at 14.1% of the amplicon library at 10.5 cm. In a similar region of the core, sequences of the *Brocadiales* group (involved in anammox by ammonia oxidation linked to nitrate/nitrite reduction [61]) were at highest sustained abundance between 5.5 and 10.5 cm (Fig. 3). All four of these groups had varying associations with modeled relative denitrification contribution. The strongest relationship was with *Brocadiales* ($R = 0.74$, $p < 0.01$), followed by *Methylomirabilaceae* ($R = 0.57$, $p < 0.01$), *Shewanellaceae* ($R = 0.53$, $p < 0.01$) and *Desulfuromondales* ($R = 0.45$, $p < 0.01$) (Supplements; Figure S5). In contrast to all of the other taxa detailed above, sequences related to the sulfate reducing *Desulfobacteraceae* [62]) were largely absent above ~10.5 cm (Fig. 3). The presence of *Desulfobacteraceae* continued below this oxic-anoxic transition to the base of the core and was closely correlated with modeled relative sulfate reduction contribution ($R = 0.88$, $p < 0.01$) (Supplements; Fig. S6).

The PCA ordination biplot provides insight into co-associations between geochemical, geomicrobial, modeled relative metabolic pathways and bioturbation datasets (Fig. 4). For example, the assemblage to the right part of the biplot is closest in ordination space to the uppermost core samples in the oxic and bioturbated zone which includes modeled and measured O_2, Arctic marine cosmopolitan aerobic marine group BD7-8, measurements of bacterial and archaeal 16S rRNA gene abundance and Mn. All organic geochemical variables (sterols, *n*-alkanes, *n*-alkanols and *n*-alkanoic acids) and $\delta^{15}N$ appear to co-vary and are grouped at the lower right part of the biplot. In contrast, *Desulfobacteraceae,* SO_4 – M, $Fe(OH)_3$ – M, TOC:N and TOC are present towards the lower left part of the biplot. To the top left of the biplot, NO_3 – M and MnO_2 – M are grouped, with *Brocadiales*, Fe, P,

Methylomirabilaceae, Desulfuromondales, Nitrosopumilaceae and *Shewanellaceae* grouped towards the top of the right quadrant. PCA axis 1 decreased from a maximum of ~2 at the top of the core clearly to a minimum of ~ −0.5 by ~7.5 cm, highlighting changes initially in indicators sensitive to the oxic interface (e.g. organic geochemistry, BD7-8, 16S archaea/bacteria), below which variance fluctuated (Supplements; Fig. S7). PCA axis 2 featured an initial peak in the oxic zone (~1.2 at 1.25 cm), a decrease (−0.2 by 4.5 cm), and then a peak to ~2 by 6.5 cm coincident with fluctuations in multiple sequenced microbial indicators, below which variance fluctuated to the base.

Discussion

We examine evidence for changes in OM reactivity with depth below the seafloor across the redox succession and assess the influence of changes in sedimentology on the reactivity of OM, to provide new insight on the coupling between geochemical and microbiological processes in Arctic shelf sea carbon cycling.

There are clear changes in bulk parameters (~10 cm) as well as biomarker distributions (~4.5 cm) in the uppermost part of the core (Fig. 1 & 2), with coincident declines in aerobic microbiological proxies (Fig. 3). Changes closest to the SWI are consistent with extensive transformations of OM in the aerobic and bioturbated sediment layer [10, 63, 64]. Below the aerobic zone, the most reactive OM has been largely consumed with clear deeper succession of microbes indicative of a transition to anoxia. This is evidenced by microbes capable of iron, manganese and nitrite dependent methane oxidation (~4.5 - 10.5 cm), transitioning at greater depth to sulfate reduction in these deeper sediments (~10.5-33 cm) where OM is less reactive (Fig. 3). Despite bioturbation levels being consistent with regional [65] and local [50] studies (i.e. maximal depth of faunal mixing ~4.3 cm), these results provide clear evidence of distinct successional redox zones transitioning with depth and associated stratification of microbial community composition [15] coupled to the diagenesis of reactive carbon, but at a reduced capacity.

i) Organic matter transformation and diagenesis below the SWI

As well as the decrease in bulk TOC and N in the uppermost ~10 cm, changes inferred by molecular organic geochemical parameters indicate a rapid decrease in the reactivity of OM

(Fig. 2). The most pronounced changes (top ~4.5 cm) are coincident with the extent of bioturbation [50]. A marked decrease in the ratio of β-sitosterol/stigmastanol can be explained by the mechanism of hydrogenation [66] and decreases in the ratio of stigmasterol/stigmastanol by reduction reactions [67]. Such reactions are also observed in the transformation and diagenesis of all sterols [68]. Although some sterols, such as β-sitosterol and stigmasterol, can be of a terrestrial plant origin [69], in this location in sediments with a mixed but mainly marine signature [31] sterols could also have a marine origin [70]. The CPI index for *n*-alkanes also shows a marked decline in the uppermost sediments, which reflects OM diagenesis as the more abundant odd chain lengths degrade [71]. This is mirrored by declines from the uppermost sample in *n*-alkanoic acid CPI_T index (where the more abundant even compounds degrade) [35] and pronounced decreases in the concentration of these compounds. Although changes in the mixing or delivery of terrestrial OM can result in changes in CPI [72], the low values in these sediments suggest a mixed, but primarily marine signature.

Coincident with CPI decreases, OEP for *n*-alkanes in the range C_{17}-C_{21} and C_{21-25} also decline, with marked changes between the sample at the SWI (~ 0.5 cm) and deeper sediment layers [37]. With decreases in OEP, OM rapidly becomes degraded and less bioavailable, a process which is most pronounced close to the SWI. Similarly, for the more labile *n*-alkanols, changes in the ratio of autochthonous to allochthonous-derived compounds [38] in the uppermost layer indicate active processing of compounds in the organic rich layer. A reverse trend in the *n*-alkanol TAR ratio probably can be explained to ~4.5 cm by dilution by more abundant short chain compounds close to the SWI, which are also less resistant to degradation than longer chain compounds [73]. However, increases to the TAR *n*-alkanol values to ~5 at ~9.5 cm could point to past deposition of OM, which appears to be reflected by increases in CPI_T for *n*-alkanoic acids and the ratio of cholesterol/brassicasterol. The pulse in TAR for *n*-alkanoic acids at ~1.75 cm suggests delivery of terrestrial material is unlikely to have been consistent and likely varied over time. Overall, the changes close to the SWI reflect the early diagenesis of lipid biomarkers observed in the oxic layer of ocean sediments [13] and are coincident with observed bioturbation zone [50], while also highlight an underlying terrestrial influence [29, 74].

Loss of TOC with depth (Fig. 1) is markedly more pronounced in the oxic layer compared with the anoxic sediments (indicated by the relative abundance of *Desulforbacteraceae,* in sequence libraries Fig. 3). For instance, TOC declines from a peak of ~1.8% close to the top

of the core at ~2.5 cm to ~1.3% by 10.5 cm at the base of the oxic zone, prior to the transitional zone indicated by *Desulforbacteraceae* (Fig. 3). Based on extrapolating the age estimation, this corresponds to a loss, given dating approximations of 3.8 x 10^{-4} % TOC per year. In marked contrast, in the established zone of anoxia from ~13.5 cm to the base, TOC declines from ~1.5 to ~1.3 over a longer time period corresponding to a loss of 8.4 x 10^{-5}% TOC per year. Although this estimation does not resolve changes in sedimentation rate and is based only on a basal age, the difference in relative TOC loss with depth corroborates changes in molecular proxies (*n*-alkanes, *n*-alkanols, sterols) which provides evidence that OM reactivity is greatest in the uppermost layer. Future changes in the relative position of the oxic/anoxic interface could lead to changes in carbon cycling driven by reactivity at the seafloor.

Both organic geochemistry (CPI *n*-alkanes, TOC, N, δ^{15}N) and measured/modeled porewater O_2 in the uppermost layers are statistically correlated with declines in the proportion of the BD7-8 marine group (Fig. 3; Supplements Fig. S2 & 3), attributed to bacterial diversity in oxic marine sedimentary environments [54] and previously detected in surface sediments of the South Atlantic Ocean [75] and the western Arctic Ocean [76]. Although more variable, 16S rRNA data show that bacteria and archaea are also only present in abundance in the uppermost 0-9.5 cm mixed layer (Fig. 3). Bacterial and archaeal richness and abundance is known to decrease exponentially with depth [77, 78] and links between organic degradation and microbial activity are particularly pronounced close to the SWI [79]. Similarly, the highest consistent levels of *Nitrosopumilaceae* (capable of ammonia oxidation to nitrite [80]) are in the uppermost sediments, correlating with lower TOC:N ratios and higher δ^{15}N indicative of microbial activity (Supplements Fig. S4). Here, ammonia oxidising archaea utilise ammonia likely generated through OM mineralisation in the sediments below which diffuse up to the bioturbated, oxic zone. The ratio of C_{15} anteiso/C_{16} FAMEs is corroborated by extensive microbial activity just below the sediment-surface interface (Fig. 2), with this compound often linked to bacterial activity as they are major constituents of bacterial membrane lipids [81] and have been detected in aquatic environments [82] including ocean sediments [83]. Peaks in the ratio of cholesterol/brassicasterol and cholesterol/β-sitosterol within the zone of bioturbation at ~2.5 cm have a similar explanation as cholesterol is a key component of bacterial membrane lipids [84]. Decreases in bulk δ^{15}N (Fig. 1) are probably explained by preferential degradation of compounds such as proteins rich in ^{15}N, deposited

493 at the SWI and subsequently degraded [64, 85], potentially sourced from under ice algal
494 blooms.
495
496 **ii) Stratification of microbes and geochemistry across the oxic to anoxic interface**
497
498 Further changes linked to the processing of OM take place below the aerobic, bioturbated
499 zone. In the aerobic to anaerobic transition zone peaks in the relative abundance of
500 bacterial taxa *Desulfuromondales* and *Shewanellaceae* from ~6.5 cm downwards indicate
501 that Fe^{3+} and Mn^{4+} reduction is taking place (Fig. 3) [86]. These taxa can utilise (reduce
502 through dissolution) metals such as Fe^{3+} and Mn^{4+} oxides as terminal electron acceptors.
503 *Shewanella spp*. are adapted to chemically stratified redox transitions [58]. Sediment Mn
504 concentrations also increase coincident with the two major peaks in *Desulfuromondales* in
505 the oxic zone, suggesting that taxa capable of metal reduction are important close to the
506 redox transition (Fig. 3). Seasonal or decadal oscillations in the delivery of OM causing the
507 position of the redox boundary to fluctuate could be a process here, potentially explaining
508 the position of Mn at the upper part of the redox boundary based on kinetics of oxidation
509 and reduction [87]. The oxic to anoxic redox transition is most clearly illustrated by the
510 marked increase of *Desulforbacteraceae* from ~10.5 cm downwards which are known sulfate
511 reducers [88] and correlates with modeled sulfate reduction (Fig. 3; Supplements Fig. S6).
512 Sulfate reducing taxa are known to persist below the oxic layer, typically also below the
513 oxidants NO_3^-, Fe^{3+} and Mn^{4+}, where they are involved in the remineralisation of organic
514 carbon [89].
515
516 Coincident with the increase in sulfate-reducing taxa at and below the oxic-anoxic transition,
517 the abundance of methane oxidizing taxa evidenced by bacteria in the group
518 *Methylomirabilaceae* peaked markedly (Fig. 3). Based on amplicon library relative
519 abundance (15%) the *Methylomirabilis* are an important group in this sequence. This family
520 have been shown to participate in anaerobic methane oxidation linked to nitrate/nitrite
521 reduction (via the generation of molecular oxygen utilised by methane monooxygenase
522 (MMO)) [90]. *Methylomirabilis* have been previously detected in ocean sediments [91], sub-
523 Arctic lake sediments [92] and are abundant in methane rich environments such as paddy
524 fields [93]. On balance, the coincidence of this group with sequences related to the
525 *Brocardiales*, which are implicated in anammox (ammonia oxidation linked to nitrate/nitrite
526 reduction [61]), may suggest involvement in ammonia oxidation. Genomic studies have
527 suggested the potential for the oxidation of ammonia by *Methylomirbilis* by use of their

oxygen dependent MMO [90] rather than by the annamox pathway involving hydrazine production [61]. Increases in TOC:N ratio in the anoxic sediments and transition zone (Fig. 3) are probably explained in this system by microbial activity utilising more N, where this is limited and more labile than C, producing OM with TOC:N ratios ~10 which gradually dilutes the lower TOC:N ratio of phytoplankton derived matter, characteristic of the uppermost layer. Additionally, if *Methylomirabilis* is acting as an ammonia oxidiser it likely produces N_2 as an inert gas, likely resulting in the gradual loss of solid phase N down the core evidenced by increases in TOC:N ratios in the anoxic sediments. Many of these bacterial taxa have the potential to be involved in multiple processes at this key transition, but denitrification (Fig. 3) also appears to be particularly important at this key transition with associations between *Methylomirbilis, Brocardiales, Desulfuromondales* and *Shewanellaceae* and modeled denitrification [29] (Supplements; Fig. S5).

iii) How does the reactivity of OM delivered to and preserved within sediments change across differences in sedimentology?

Fine particulates (silty clays) are abundant close to the SWI (Fig. 1), together with biomarkers which infer more reactive OM such as high CPI and $OEP_{(17\text{-}21\ \&\ 21\text{-}25)}$ for *n*-alkanes, high ratios of stigmasterol/stigmastanol and β-sitosterol/stigmastanol, plus high total alkanoic acids (Fig. 2). Close to the SWI the weaker bonds of more reactive organic components may continue to be attached and the fine particulate (clay-like) minerals may help, in part entrain, enmesh or adsorb organics in a mineral matrix [94]. The coarser fraction immediately beneath from ~0.75 until 2.5 cm could be associated with bioturbation sorting and be a particle capture layer [95], immediately below the most intensive reworking zone. Finer particles from ~2.5 to 5.5 cm remain within the maximum bioturbation zone, with these size classes potentially supporting capture of microbially influenced biomarkers (e.g. pulses of C_{15} anteiso:16:0 FAMEs and cholesterol:brassicasterol ratios, Fig. 2) when evidence of microbial activity (e.g. 16s RNA archaea, Fig. 3) is high.

The transition to finer particulates peaking at ~14.5 cm, which is accompanied by increases in Fe and P (Fig. 1) could be a sediment deposition event similar to scenarios across the Barents Sea. Although the specific underlying mechanism driving this potential deposition cannot be disentangled from this evidence, possibilities include regional transport from land [96], cross-shelf transport [97] or accumulations linked to seasonal redox oscillations [87].

We might expect organic biomarker evidence of either source (e.g. terrestrial input) or reactivity changes to be coeval with this change in sedimentology, but there is little evidence of response at similar magnitudes to OM transformations at the SWI. Slight fluctuations in *n*-alkane CPI at ~17.5 cm and $OEP_{17\text{-}21}$ at ~15.5 cm (Fig. 2) could indicate slightly more reactive organics is being preserved in finer particulates, but the response is minor and offset slightly from changes in grain size. Since the change in sedimentology does not have a clear link with reactivity of OM evidenced by bulk parameters (TOC, N, TOC:N ratio) or biomarker distributions (*n*-alkanes, *n*-alkanols or sterol ratios) then this suggests the change in sedimentology was either not accompanied by significant organic material, or processes at the SWI have removed any noticeable geochemical signatures. Previous studies suggest the material released from ice sheets and glaciers are sources of quickly processed highly reactive OM [98, 99]. Potential reactive material, which may have been brought into the system during past disturbances or reworking may have been subsequently degraded, and does not continue to exert a major impact on OM cycling (evidenced by extractable lipid fractions), except by potentially supporting in part, microbial taxa capable of using metals for respiration *(Shewanellaceae* and *Desulfuromondales*, Fig. 3*).* The Mn and Fe changes in sedimentology (Mn peak is shallower) may be offset due to different kinetics of oxidation and reduction between oxides of these compounds [87] and these microbes may also be sensitive to porewater diffusion of metals.

iv) The role of coupled microbial and geochemical studies for understanding carbon cycling in Arctic shelf systems

Clear separation between indicators of OM reactivity, microbial communities at the redox interface and indicators of sulfate reduction processes in the PCA biplot (Fig. 4), which vary across the redox profile (Supplements; Figure S7), highlights the coupled relationships between a multiplicity of complementary but competing processes which stratify according to depth. This clear separation supports close relationships between geochemical variables (e.g. CPI *n*-alkanes, $\delta^{15}N$, %N, %TOC) and O_2, beneath which across the oxic to anoxic transition microbes involved in multiple processes stratify (denitrification, nitrite production and iron/manganese reduction etc.), prior to evidence of sulfate reduction below the transition to depth (Supplements; Fig. S2 - 6).

This detailed geochemistry and microbiology study provides a coupled framework with wider sedimentary processes including porewater geochemistry (from reactive transport

modelling and measured O_2 [29]) and bioturbation [50], consistent with expectations for a continental shelf system [100]. The extent of successional redox associated processes controlling the cycling of carbon in sediments at and below the SWI is coupled closely to the environmental setting (Barents Sea continental shelf) and is likely to be sensitive to future changes, especially those driven by atmospheric and oceanic warming. The trends in OM transformations and redox succession observed at B15 are likely to be typical of shelf environments with similar water depth, sediment type, overlying water masses and levels of primary production and carbon export. Specifically, although this study focuses on one station (B15) it is possible to suggest, broadly that this station may be representative of wider regional processes. In terms of surface sediment particle size in the Barents Sea, this station is consistent with locations in a southerly direction south (to ~ 75 °N) [101] and so profiles may be similar across a wider part of the continental shelf. If upscaled, this study would demonstrate there is a key pool of reactive OM dependent on microbial control, making up part of the more reactive carbon burial component which could be lost from this key store if the redox interface was shallower. This scenario is possible as changes in OM supply are likely to adjust with future changes in ocean stratification and sea-ice retreat [25].

Future studies should follow a similar approach to assess how the depth and extent of redox sensitive successional processes might be affected by geographical position across Arctic continental shelves (e.g. Chukchi Sea, Bering Sea, East Siberian Sea, Laptev Sea). Comparisons of profiles will be particularly insightful to help understand how changes to the Arctic including sea ice losses and associated changes in water column vertical mixing [25, 102] are influencing ocean primary productivity in the Arctic [5], which is tightly coupled to carbon fluxes reaching the seafloor [9]. Such studies will assess the stability and bioavailability of carbon sequestered as organic carbon burial is the principal mechanism for long-term carbon sequestration [7, 8], which ultimately becomes part of the permanent geological record [9].

Conclusions

Our study demonstrates mechanistic links between microbial processing and changes in organic and inorganic parameters across the oxic to anoxic interface are distinct, but interactive and tightly coupled to biological mixing and the reactivity of OM. Specifically we found:

i) Distinct links between aerobic processes, reactive carbon and highest abundances of bacteria and archaea in the uppermost layer (0-4.5 cm), coincident with the extent of biological mixing and changes in the reactivity of OM (indicated by *n*-alkanes, *n*-alkanols, *n*-alkanoic acids and sterols).

ii) A dominance of microbes involved in nitrate/nitrite and iron/manganese reduction across the oxic-anoxic redox boundary (~4.5-10.5 cm), with convincing denitrification relationships confirming this key intermediate zone.

iii) Sulfate reducers dominate in deeper anoxic sediments which is consistent with OM transformations and biological reworking, but that deeper changes in sedimentology have only minor effects on the reactivity of organic carbon (compared with at the SWI), probably due to past processing.

Future research should compare coupled geochemistry-microbial profiles between ice-covered and ice-free zones of the Arctic to elucidate linkages between ice cover and microbial processing of OM at the seafloor. This is especially pertinent and should be coupled with estimates of carbon burial in different locations across the Barents Sea, given the trend for increasing oceanographic changes in this region [25].

Additional Information

Acknowledgments

Appreciation is given to the excellent support provided by the crew and science parties on board the RRS James Clark Ross (JR16006) including shipboard facilities (NOC & BAS) and PSO Jo Hopkins. We thank Heather Birch and Timothy Knowles for assistance with ^{14}C-AMS dating of foraminifera, Martin Solan for provision of bioturbation metrics and Jeff Peakcall for providing access to a grain size analyser. We appreciate technical assistance from Darren Gröcke (IRMS), Bernard Bowler (EA), Alex Charlton (TOC) and Paul Donohoe (GC-MS). We are grateful for the comments from the reviewers, which helped improve the manuscript.

Funding Statement

This work resulted from the ChAOS project (NE/P00637X/1; NE/P006493/1; NE/P006108/1; NE/P005942/1) part of the Changing Arctic Ocean programme, funded by UKRI Natural Environment Research Council (NERC).

Data Accessibility

Data used in this study is available in the supplements.

Competing Interests

We have no competing interests

Authors' Contributions

M.A.S. wrote the manuscript initial draft, conducted fieldwork/sampling, compiled datasets and carried out bulk and organic geochemical analyses. J.C.F. provided inorganic XRF data, conducted fieldwork/sampling, contributed ideas on sedimentology and to the initial manuscript. L.L.A. carried out microbiological analyses. F.S.F. advised on suitable organic geochemical techniques and provided insight into OM reactivity. N.D.G. designed microbiological approach and contributed key ideas on redox stratification to initial manuscript. K.T. carried out quantitative 16S rRNA analyses and co-designed microbiological approach. K.R.H project managed ^{14}C radiocarbon analyses. R.G.H carried out $\delta^{15}N$ analyses with M.A.S. and advised on geochemical sampling strategy. S.F.H. & A.T. carried out fieldwork & porewater nutrient analysis which underpins model comparison. P.L. carried out bioinformatics and constructed sequencing pipeline. S.P. carried out ^{14}C analyses on foraminifera. A.F. carried out grain size analysis. C.M. conducted fieldwork/sampling, advised on sedimentology and project managed inorganic geochemical aspects. G.D.A. contributed early ideas, revised the initial manuscript and project managed organic geochemical aspects. All authors commented on the manuscript and approved the final submission.

689 # References

[1] LaRowe, D. E., Arndt, S., Bradley, J. A., Estes, E. R., Hoarfrost, A., Lang, S. Q., Lloyd, K. G., Mahmoudi, N., Orsi, W. D., Shah Walter, S. R., et al. 2020 The fate of organic carbon in marine sediments - New insights from recent data and analysis. *Earth-Sci. Rev.* **204**, 103146. (DOI:10.1016/j.earscirev.2020.103146).
[2] Bourgeois, S., Archambault, P. & Witte, U. 2017 Organic matter remineralization in marine sediments: A Pan-Arctic synthesis. *Global Biogeochemical Cycles* **31**, 190-213. (DOI:10.1002/2016gb005378).
[3] Ravenschlag, K., Sahm, K., Pernthaler, J. & Amann, R. 1999 High Bacterial Diversity in Permanently Cold Marine Sediments. *Appl. Environ. Microbiol.* **65**, 3982-3989.
[4] Renaud, P. E., Sejr, M. K., Bluhm, B. A., Sirenko, B. & Ellingsen, I. H. 2015 The future of Arctic benthos: Expansion, invasion, and biodiversity. *Prog. Oceanogr.* **139**, 244-257. (DOI:10.1016/j.pocean.2015.07.007).
[5] Arrigo, K. R. & van Dijken, G. L. 2015 Continued increases in Arctic Ocean primary production. *Prog. Oceanogr.* **136**, 60-70. (DOI:10.1016/j.pocean.2015.05.002).
[6] Boetius, A., Albrecht, S., Bakker, K., Bienhold, C., Felden, J., Fernández-Méndez, M., Hendricks, S., Katlein, C., Lalande, C., Krumpen, T., et al. 2013 Export of Algal Biomass from the Melting Arctic Sea Ice. *Science* **339**, 1430-1432. (DOI:10.1126/science.1231346).
[7] Smith, R. W., Bianchi, T. S., Allison, M., Savage, C. & Galy, V. 2015 High rates of organic carbon burial in fjord sediments globally. *Nature Geoscience* **8**, 450-453. (DOI:10.1038/ngeo2421).
[8] Hedges, J. I., Keil, R. G. & Benner, R. 1997 What happens to terrestrial organic matter in the ocean? *Organic Geochemistry* **27**, 195-212. (DOI:10.1016/S0146-6380(97)00066-1).
[9] Stein, R., Macdonald, R. W., Stein, R. & MacDonald, R. W. 2004 The organic carbon cycle in the Arctic Ocean.
[10] Wakeham, S. G. & Canuel, E. A. 2006 Degradation and Preservation of Organic Matter in Marine Sediments. In *Marine Organic Matter: Biomarkers, Isotopes and DNA* (ed. J. K. Volkman), pp. 295-321. Berlin, Heidelberg, Springer Berlin Heidelberg.
[11] Arndt, S., Jørgensen, B. B., LaRowe, D. E., Middelburg, J. J., Pancost, R. D. & Regnier, P. 2013 Quantifying the degradation of organic matter in marine sediments: A review and synthesis. *Earth-Sci. Rev.* **123**, 53-86. (DOI:10.1016/j.earscirev.2013.02.008).
[12] Zonneveld, K. A. F., Versteegh, G. J. M., Kasten, S., Eglinton, T. I., Emeis, K. C., Huguet, C., Koch, B. P., de Lange, G. J., de Leeuw, J. W., Middelburg, J. J., et al. 2010 Selective preservation of organic matter in marine environments; processes and impact on the sedimentary record. *Biogeosciences* **7**, 483-511. (DOI:10.5194/bg-7-483-2010).
[13] Madureira, L. A. S., Conte, M. H. & Eglinton, G. 1995 Early diagenesis of lipid biomarker compounds in North Atlantic sediments. *Paleoceanography* **10**, 627-642. (DOI:10.1029/94pa03299).
[14] Ravenschlag, K., Sahm, K. & Amann, R. 2001 Quantitative Molecular Analysis of the Microbial Community in Marine Arctic Sediments (Svalbard). *Appl. Environ. Microbiol.* **67**, 387-395. (DOI:10.1128/aem.67.1.387-395.2001).
[15] Jorgensen, S. L., Hannisdal, B., Lanzén, A., Baumberger, T., Flesland, K., Fonseca, R., Øvreås, L., Steen, I. H., Thorseth, I. H., Pedersen, R. B., et al. 2012 Correlating microbial community profiles with geochemical data in highly stratified sediments from the Arctic Mid-Ocean Ridge. *Proceedings of the National Academy of Sciences* **109**, E2846-E2855. (DOI:10.1073/pnas.1207574109).
[16] Algora, C., Gründger, F., Adrian, L., Damm, V., Richnow, H.-H. & Krüger, M. 2013 Geochemistry and Microbial Populations in Sediments of the Northern Baffin Bay, Arctic. *Geomicrobiol. J.* **30**, 690-705. (DOI:10.1080/01490451.2012.758195).
[17] Jones, J. G. 1985 Microbes and microbial processes in sediments. *Philosophical Transactions of the Royal Society of London. Series A, Mathematical and Physical Sciences* **315**, 3-17. (DOI:10.1098/rsta.1985.0025).

[18] van der Weijden, C. H., Reichart, G. J. & Visser, H. J. 1999 Enhanced preservation of organic matter in sediments deposited within the oxygen minimum zone in the northeastern Arabian Sea. *Deep Sea Research Part I: Oceanographic Research Papers* **46**, 807-830. (DOI:10.1016/S0967-0637(98)00093-4).
[19] Onarheim, I. H. & Årthun, M. 2017 Toward an ice-free Barents Sea. *Geophysical Research Letters* **44**, 8387-8395. (DOI:10.1002/2017gl074304).
[20] Serreze, M. C., Holland, M. M. & Stroeve, J. 2007 Perspectives on the Arctic's Shrinking Sea-Ice Cover. *Science* **315**, 1533-1536. (DOI:10.1126/science.1139426).
[21] Stroeve, J. C., Kattsov, V., Barrett, A., Serreze, M., Pavlova, T., Holland, M. & Meier, W. N. 2012 Trends in Arctic sea ice extent from CMIP5, CMIP3 and observations. *Geophysical Research Letters* **39**, 1-7. (DOI:10.1029/2012GL052676).
[22] Serreze, M. C. & Barry, R. G. 2011 Processes and impacts of Arctic amplification: A research synthesis. *Global Planet. Change* **77**, 85-96. (DOI:10.1016/j.gloplacha.2011.03.004).
[23] Polyakov, I. V., Pnyushkov, A. V., Alkire, M. B., Ashik, I. M., Baumann, T. M., Carmack, E. C., Goszczko, I., Guthrie, J., Ivanov, V. V., Kanzow, T., et al. 2017 Greater role for Atlantic inflows on sea-ice loss in the Eurasian Basin of the Arctic Ocean. *Science* **356**, 285-291. (DOI:10.1126/science.aai8204).
[24] Ardyna, M., Babin, M., Gosselin, M., Devred, E., Rainville, L. & Tremblay, J.-É. 2014 Recent Arctic Ocean sea ice loss triggers novel fall phytoplankton blooms. *Geophysical Research Letters* **41**, 6207-6212. (DOI:10.1002/2014gl061047).
[25] Lind, S., Ingvaldsen, R. B. & Furevik, T. 2018 Arctic warming hotspot in the northern Barents Sea linked to declining sea-ice import. *Nature Climate Change* **8**, 634-639. (DOI:10.1038/s41558-018-0205-y).
[26] Jacob, M., Soltwedel, T., Boetius, A. & Ramette, A. 2013 Biogeography of Deep-Sea Benthic Bacteria at Regional Scale (LTER HAUSGARTEN, Fram Strait, Arctic). *PloS one* **8**, e72779. (DOI:10.1371/journal.pone.0072779).
[27] Algora, C., Vasileiadis, S., Wasmund, K., Trevisan, M., Krüger, M., Puglisi, E. & Adrian, L. 2015 Manganese and iron as structuring parameters of microbial communities in Arctic marine sediments from the Baffin Bay. *FEMS Microbiol. Ecol.* **91**. (DOI:10.1093/femsec/fiv056).
[28] Bienhold, C., Boetius, A. & Ramette, A. 2012 The energy–diversity relationship of complex bacterial communities in Arctic deep-sea sediments. *The ISME Journal* **6**, 724-732. (DOI:10.1038/ismej.2011.140).
[29] Freitas, F. S., Hendry, K. R., Henley, S. F., Faust, J. C., Tessin, A. C., Stevenson, M. A., Abbott, G. D., März, C. & Arndt, S. 2020 Benthic-pelagic coupling in the Barents Sea: an integrated data-model framework. *Philosophical Transactions of the Royal Society A*.
[30] Hopkins, J. 2018 The Changing Arctic Ocean Cruise JR16006. In *RRS James Clark Ross Cruise Report No. 51 30 June - 8 August 2017* (Liverpool, National Oceanography Centre.
[31] Stevenson, M. A. & Abbott, G. D. 2019 Exploring the composition of macromolecular organic matter in Arctic Ocean sediments under a changing sea ice gradient. *Journal of Analytical and Applied Pyrolysis* **140**, 102-111. (DOI:10.1016/j.jaap.2019.02.006).
[32] Fetterer, F., Knowles, K., Meier, W., Savoie, M. & Windnagel, A. 2017 Updated daily. Sea Ice Index, Version 3, Boulder, Colorado USA. NSIDC: National Snow and Ice Data Center. (
[33] Holtvoeth, J., Vogel, H., Wagner, B. & Wolff, G. A. 2010 Lipid biomarkers in Holocene and glacial sediments from ancient Lake Ohrid (Macedonia, Albania). *Biogeosciences* **7**, 3473-3489. (DOI:10.5194/bg-7-3473-2010).
[34] Bourbonniere, R. A. & Meyers, P. A. 1996 Sedimentary geolipid records of historical changes in the watersheds and productivities of Lakes Ontario and Erie. *Limnology and Oceanography* **41**, 352-359. (DOI:10.4319/lo.1996.41.2.0352).
[35] Matsuda, H. & Koyama, T. 1977 Early diagenesis of fatty acids in lacustrine sediments—II. A statistical approach to changes in fatty acid composition from recent sediments and some source materials. *Geochimica et Cosmochimica Acta* **41**, 1825-1834. (DOI:10.1016/0016-7037(77)90214-9).

[36] Bray, E. E. & Evans, E. D. 1961 Distribution of *n*-paraffins as a clue to recognition of source beds. *Geochimica et Cosmochimica Acta* **22**, 2-15. (DOI:10.1016/0016-7037(61)90069-2).
[37] Scalan, E. S. & Smith, J. E. 1970 An improved measure of the odd-even predominance in the normal alkanes of sediment extracts and petroleum. *Geochimica et Cosmochimica Acta* **34**, 611-620. (DOI:10.1016/0016-7037(70)90019-0).
[38] Pearson, E. J., Farrimond, P. & Juggins, S. 2007 Lipid geochemistry of lake sediments from semi-arid Spain: Relationships with source inputs and environmental factors. *Organic Geochemistry* **38**, 1169-1195. (DOI:10.1016/j.orggeochem.2007.02.007).
[39] Kozich, J. J., Westcott, S. L., Baxter, N. T., Highlander, S. K. & Schloss, P. D. 2013 Development of a Dual-Index Sequencing Strategy and Curation Pipeline for Analyzing Amplicon Sequence Data on the MiSeq Illumina Sequencing Platform. *Appl. Environ. Microbiol.* **79**, 5112-5120. (DOI:10.1128/aem.01043-13).
[40] Caporaso, J. G., Lauber, C. L., Walters, W. A., Berg-Lyons, D., Lozupone, C. A., Turnbaugh, P. J., Fierer, N. & Knight, R. 2011 Global patterns of 16S rRNA diversity at a depth of millions of sequences per sample. *Proceedings of the National Academy of Sciences* **108**, 4516-4522. (DOI:10.1073/pnas.1000080107).
[41] Bolyen, E. & Rideout, J. R. & Dillon, M. R. & Bokulich, N. A. & Abnet, C. C. & Al-Ghalith, G. A. & Alexander, H. & Alm, E. J. & Arumugam, M. & Asnicar, F., et al. 2019 Reproducible, interactive, scalable and extensible microbiome data science using QIIME 2. *Nat. Biotechnol.* **37**, 852-857. (DOI:10.1038/s41587-019-0209-9).
[42] Callahan, B. J., McMurdie, P. J., Rosen, M. J., Han, A. W., Johnson, A. J. A. & Holmes, S. P. 2016 DADA2: High-resolution sample inference from Illumina amplicon data. *Nat. Methods* **13**, 581-583. (DOI:10.1038/nmeth.3869).
[43] Quast, C., Pruesse, E., Yilmaz, P., Gerken, J., Schweer, T., Yarza, P., Peplies, J. & Glöckner, F. O. 2012 The SILVA ribosomal RNA gene database project: improved data processing and web-based tools. *Nucleic Acids Res.* **41**, D590-D596. (DOI:10.1093/nar/gks1219).
[44] Ovreås, L., Forney, L., Daae, F. L. & Torsvik, V. 1997 Distribution of bacterioplankton in meromictic Lake Saelenvannet, as determined by denaturing gradient gel electrophoresis of PCR-amplified gene fragments coding for 16S rRNA. *Appl. Environ. Microbiol.* **63**, 3367-3373.
[45] Suzuki, M. T., Taylor, L. T. & DeLong, E. F. 2000 Quantitative Analysis of Small-Subunit rRNA Genes in Mixed Microbial Populations via 5′-Nuclease Assays. *Appl. Environ. Microbiol.* **66**, 4605-4614. (DOI:10.1128/aem.66.11.4605-4614.2000).
[46] Currie, A. R., Tait, K., Parry, H., de Francisco-Mora, B., Hicks, N., Osborn, A. M., Widdicombe, S. & Stahl, H. 2017 Marine Microbial Gene Abundance and Community Composition in Response to Ocean Acidification and Elevated Temperature in Two Contrasting Coastal Marine Sediments. *Frontiers in Microbiology* **8**. (DOI:10.3389/fmicb.2017.01599).
[47] Tuna, T., Fagault, Y., Bonvalot, L., Capano, M. & Bard, E. 2018 Development of small CO2 gas measurements with AixMICADAS. *Nuclear Instruments and Methods in Physics Research Section B: Beam Interactions with Materials and Atoms* **437**, 93-97. (DOI:10.1016/j.nimb.2018.09.012).
[48] Lougheed, B. & Obrochta, S. 2016 MatCal: Open source Bayesian 14 C age calibration in MatLab. *Journal of Open Research Software* **4**. (DOI:doi.org/10.5334/jors.130).
[49] Baskaran, M., Bianchi, T. S. & Filley, T. R. 2017 Inconsistencies between 14C and short-lived radionuclides-based sediment accumulation rates: Effects of long-term remineralization. *J. Environ. Radioact.* **174**, 10-16. (DOI:10.1016/j.jenvrad.2016.07.028).
[50] Solan, M., Ward, E. R., Wood, C. L., Reed, A. J., Grange, L. J. & Godbold, J. A. 2020 Climate driven benthic invertebrate activity and biogeochemical functioning across the Barents Sea Polar Front. *Philosophical Transactions of the Royal Society A*.
[51] Solan, M., Wigham, B., D., Hudson, I., R. , Kennedy, R., Coulon, C., H. , Norling, K., Nilsson, H., C. & Rosenberg, R. 2004 In situ quantification of bioturbation using time lapse fluorescent sediment profile imaging (f SPI), luminophore tracers and model simulation. *Mar. Ecol. Prog. Ser.* **271**, 1-12. (DOI:10.3354/meps271001).

[52] Hale, R., Mavrogordato, M. N., Tolhurst, T. J. & Solan, M. 2014 Characterizations of how species mediate ecosystem properties require more comprehensive functional effect descriptors. *Scientific Reports* **4**, 6463. (DOI:10.1038/srep06463).
[53] Ter Braak, C. & Smilauer, P. 2002 Canoco for Windows version 4.5. *Biometris–Plant Research International, Wageningen*.
[54] Li, L., Kato, C. & Horikoshi, K. 1999 Bacterial diversity in deep-sea sediments from different depths. *Biodiversity & Conservation* **8**, 659-677. (DOI:10.1023/a:1008848203739).
[55] Dyksma, S., Bischof, K., Fuchs, B. M., Hoffmann, K., Meier, D., Meyerdierks, A., Pjevac, P., Probandt, D., Richter, M., Stepanauskas, R., et al. 2016 Ubiquitous Gammaproteobacteria dominate dark carbon fixation in coastal sediments. *The ISME Journal* **10**, 1939-1953. (DOI:10.1038/ismej.2015.257).
[56] Meyer, J., Akerman, N., Proskurowski, G. & Huber, J. 2013 Microbiological characterization of post-eruption "snowblower" vents at Axial Seamount, Juan de Fuca Ridge. *Frontiers in Microbiology* **4**. (DOI:10.3389/fmicb.2013.00153).
[57] Qin, W., Martens-Habbena, W., Kobelt, J. N. & Stahl, D. A. 2015 *Candidatus* nitrosopumilus. *Bergey's Manual of Systematics of Archaea and Bacteria*, 1-9. (DOI:10.1002/9781118960608.gbm01290).
[58] Fredrickson, J. K., Romine, M. F., Beliaev, A. S., Auchtung, J. M., Driscoll, M. E., Gardner, T. S., Nealson, K. H., Osterman, A. L., Pinchuk, G., Reed, J. L., et al. 2008 Towards environmental systems biology of Shewanella. *Nature Reviews Microbiology* **6**, 592-603. (DOI:10.1038/nrmicro1947).
[59] Coates, J. D., Lonergan, D. J., Philips, E. J. P., Jenter, H. & Lovley, D. R. 1995 Desulfuromonas palmitatis sp. nov., a marine dissimilatory Fe(III) reducer that can oxidize long-chain fatty acids. *Arch. Microbiol.* **164**, 406-413. (DOI:10.1007/BF02529738).
[60] Wu, M. L., de Vries, S., van Alen, T. A., Butler, M. K., Op den Camp, H. J. M., Keltjens, J. T., Jetten, M. S. M. & Strous, M. 2011 Physiological role of the respiratory quinol oxidase in the anaerobic nitrite-reducing methanotroph 'Candidatus Methylomirabilis oxyfera'. *Microbiology* **157**, 890-898. (DOI:10.1099/mic.0.045187-0).
[61] Kuenen, J. G. 2008 Anammox bacteria: from discovery to application. *Nature Reviews Microbiology* **6**, 320-326. (DOI:10.1038/nrmicro1857).
[62] Kuever, J., Rainey, F. & Widdel, F. 2014 The family desulfobacteraceae. In *The Prokaryotes: Deltaproteobacteria and Epsilonproteobacteria* (eds. E. Rosenberg, E. DeLong, S. Lory, E. Stackebrandt & F. Thompson), pp. 45-73, Springer Berlin Heidelberg.
[63] Middelburg, J. J. 2018 Review and syntheses: to the bottom of carbon processing at the seafloor. *Biogeosciences* **15**, 413-427. (DOI:10.5194/bg-15-413-2018).
[64] Freudenthal, T., Wagner, T., Wenzhöfer, F., Zabel, M. & Wefer, G. 2001 Early diagenesis of organic matter from sediments of the eastern subtropical Atlantic: evidence from stable nitrogen and carbon isotopes. *Geochimica et Cosmochimica Acta* **65**, 1795-1808. (DOI:10.1016/S0016-7037(01)00554-3).
[65] Oleszczuk, B., Michaud, E., Morata, N., Renaud, P. E. & Kędra, M. 2019 Benthic macrofaunal bioturbation activities from shelf to deep basin in spring to summer transition in the Arctic Ocean. *Mar. Environ. Res.* **150**, 104746. (DOI:10.1016/j.marenvres.2019.06.008).
[66] Saxena, P. B. 2007 *Chemistry of Alkaloids*. Delhi, Discovery Publishing House.
[67] Crompton, D. W. T., Crompton, D. W. T. & Nickol, B. B. 1985 *Biology of the Acanthocephala*, Cambridge University Press.
[68] Abbott, G. D., Lewis, C. A., Maxwell, J. R., Durand, B., Mackenzie, A. S., McKenzie, D. P., Beaumont, C., Eglinton, G., Curtis, C. D., McKenzie, D. P., et al. 1985 The kinetics of specific organic reactions in the zone of catagenesis. *Philosophical Transactions of the Royal Society of London. Series A, Mathematical and Physical Sciences* **315**, 107-122. (DOI:doi:10.1098/rsta.1985.0032).
[69] Wen-Yen, H. & Meinschein, W. G. 1976 Sterols as source indicators of organic materials in sediments. *Geochimica et Cosmochimica Acta* **40**, 323-330. (DOI:10.1016/0016-7037(76)90210-6).

[70] Yunker, M. B., Belicka, L. L., Harvey, H. R. & Macdonald, R. W. 2005 Tracing the inputs and fate of marine and terrigenous organic matter in Arctic Ocean sediments: A multivariate analysis of lipid biomarkers. *Deep Sea Research Part II: Topical Studies in Oceanography* **52**, 3478-3508. (DOI:10.1016/j.dsr2.2005.09.008).
[71] Bianchi, T. S. & Canuel, E. A. 2011 *Chemical biomarkers in aquatic ecosystems*, Princeton University Press.
[72] Vonk, J. E., van Dongen, B. E. & Gustafsson, Ö. 2008 Lipid biomarker investigation of the origin and diagenetic state of sub-arctic terrestrial organic matter presently exported into the northern Bothnian Bay. *Marine Chemistry* **112**, 1-10. (DOI:10.1016/j.marchem.2008.07.001).
[73] Meyers, P. A. 1997 Organic geochemical proxies of paleoceanographic, paleolimnologic, and paleoclimatic processes. *Organic Geochemistry* **27**, 213-250. (DOI:10.1016/S0146-6380(97)00049-1).
[74] Pathirana, I., Knies, J., Felix, M. & Mann, U. 2014 Towards an improved organic carbon budget for the western Barents Sea shelf. *Clim. Past* **10**, 569-587. (DOI:10.5194/cp-10-569-2014).
[75] Schauer, R., Bienhold, C., Ramette, A. & Harder, J. 2010 Bacterial diversity and biogeography in deep-sea surface sediments of the South Atlantic Ocean. *The ISME Journal* **4**, 159-170. (DOI:10.1038/ismej.2009.106).
[76] Han, D., Kang, I., Ha, H. K., Kim, H. C., Kim, O.-S., Lee, B. Y., Cho, J.-C., Hur, H.-G. & Lee, Y. K. 2014 Bacterial Communities of Surface Mixed Layer in the Pacific Sector of the Western Arctic Ocean during Sea-Ice Melting. *PLOS ONE* **9**, e86887. (DOI:10.1371/journal.pone.0086887).
[77] Lipp, J. S., Morono, Y., Inagaki, F. & Hinrichs, K.-U. 2008 Significant contribution of Archaea to extant biomass in marine subsurface sediments. *Nature* **454**, 991-994. (DOI:10.1038/nature07174).
[78] Parkes, R. J., Cragg, B. A. & Wellsbury, P. 2000 Recent studies on bacterial populations and processes in subseafloor sediments: A review. *HydJ* **8**, 11-28. (DOI:10.1007/pl00010971).
[79] Walsh, E. A., Kirkpatrick, J. B., Pockalny, R., Sauvage, J., Spivack, A. J., Murray, R. W., Sogin, M. L. & D'Hondt, S. 2016 Relationship of Bacterial Richness to Organic Degradation Rate and Sediment Age in Subseafloor Sediment. *Appl. Environ. Microbiol.* **82**, 4994-4999. (DOI:10.1128/aem.00809-16).
[80] Könneke, M., Bernhard, A. E., de la Torre, J. R., Walker, C. B., Waterbury, J. B. & Stahl, D. A. 2005 Isolation of an autotrophic ammonia-oxidizing marine archaeon. *Nature* **437**, 543-546. (DOI:10.1038/nature03911).
[81] Kaneda, T. 1991 Iso- and anteiso-fatty acids in bacteria: biosynthesis, function, and taxonomic significance. *Microbiological Reviews* **55**, 288-302.
[82] Zou, L., Wang, X.-C., Callahan, J., Culp, R. A., Chen, R. F., Altabet, M. A. & Sun, M.-Y. 2004 Bacterial roles in the formation of high-molecular-weight dissolved organic matter in estuarine and coastal waters: Evidence from lipids and the compound-specific isotopic ratios. *Limnology and Oceanography* **49**, 297-302. (DOI:10.4319/lo.2004.49.1.0297).
[83] Cooper, W. J. & Blumer, M. 1968 Linear, iso and anteiso fatty acids in recent sediments of the North Atlantic. *Deep Sea Research and Oceanographic Abstracts* **15**, 535-540. (DOI:10.1016/0011-7471(68)90062-4).
[84] Sáenz, J. P., Grosser, D., Bradley, A. S., Lagny, T. J., Lavrynenko, O., Broda, M. & Simons, K. 2015 Hopanoids as functional analogues of cholesterol in bacterial membranes. *Proceedings of the National Academy of Sciences* **112**, 11971-11976. (DOI:10.1073/pnas.1515607112).
[85] Nakatsuka, T., Handa, N., Harada, N., Sugimoto, T. & Imaizumi, S. 1997 Origin and decomposition of sinking particulate organic matter in the deep water column inferred from the vertical distributions of its $\delta^{15}N$, δ^{13} and δ^{14}. *Deep Sea Research Part I: Oceanographic Research Papers* **44**, 1957-1979. (DOI:10.1016/S0967-0637(97)00051-4).
[86] Di Christina, T. J. & De Long, E. F. 1993 Design and application of rRNA-targeted oligonucleotide probes for the dissimilatory iron- and manganese-reducing bacterium Shewanella putrefaciens. *Appl. Environ. Microbiol.* **59**, 4152-4160.

[87] Gobeil, C., Macdonald, R. W. & Sundby, B. 1997 Diagenetic separation of cadmium and manganese in suboxic continental margin sediments. *Geochimica et Cosmochimica Acta* **61**, 4647-4654. (DOI:10.1016/S0016-7037(97)00255-X).
[88] Buongiorno, J., Herbert, L. C., Wehrmann, L. M., Michaud, A. B., Laufer, K., Røy, H., Jørgensen, B. B., Szynkiewicz, A., Faiia, A., Yeager, K. M., et al. 2019 Complex Microbial Communities Drive Iron and Sulfur Cycling in Arctic Fjord Sediments. *Appl. Environ. Microbiol.* **85**, e00949-00919. (DOI:10.1128/aem.00949-19).
[89] Llobet-Brossa, E., Rabus, R., Böttcher, M. E., Könneke, M., Finke, N., Schramm, A., Meyer, R. L., Grötzschel, S., Rosselló-Mora, R. & Amann, R. 2002 Community structure and activity of sulfate-reducing bacteria in an intertidal surface sediment: a multi-method approach. *Aquat. Microb. Ecol.* **29**, 211-226. (DOI:10.3354/ame029211).
[90] Versantvoort, W., Guerrero-Cruz, S., Speth, D. R., Frank, J., Gambelli, L., Cremers, G., van Alen, T., Jetten, M. S. M., Kartal, B., Op den Camp, H. J. M., et al. 2018 Comparative Genomics of Candidatus Methylomirabilis Species and Description of Ca. Methylomirabilis Lanthanidiphila. *Frontiers in Microbiology* **9**. (DOI:10.3389/fmicb.2018.01672).
[91] Chen, J., Jiang, X.-W. & Gu, J.-D. 2015 Existence of Novel Phylotypes of Nitrite-Dependent Anaerobic Methane-Oxidizing Bacteria in Surface and Subsurface Sediments of the South China Sea. *Geomicrobiol. J.* **32**, 1-10. (DOI:10.1080/01490451.2014.917742).
[92] Martinez-Cruz, K., Leewis, M.-C., Herriott, I. C., Sepulveda-Jauregui, A., Anthony, K. W., Thalasso, F. & Leigh, M. B. 2017 Anaerobic oxidation of methane by aerobic methanotrophs in sub-Arctic lake sediments. *Sci. Total Environ.* **607-608**, 23-31. (DOI:10.1016/j.scitotenv.2017.06.187).
[93] Zhou, L., Wang, Y., Long, X.-E., Guo, J. & Zhu, G. 2014 High abundance and diversity of nitrite-dependent anaerobic methane-oxidizing bacteria in a paddy field profile. *FEMS Microbiol. Lett.* **360**, 33-41. (DOI:10.1111/1574-6968.12567).
[94] Mayer, L. M. 1993 Organic Matter at the Sediment-Water Interface. In *Organic Geochemistry: Principles and Applications* (eds. M. H. Engel & S. A. Macko), pp. 171-184. Boston, MA, Springer US.
[95] Aller, R. C. & Cochran, J. K. 2019 The Critical Role of Bioturbation for Particle Dynamics, Priming Potential, and Organic C Remineralization in Marine Sediments: Local and Basin Scales. *Frontiers in Earth Science* **7**. (DOI:10.3389/feart.2019.00157).
[96] Rasmussen, T. L. & Thomsen, E. 2013 Pink marine sediments reveal rapid ice melt and Arctic meltwater discharge during Dansgaard–Oeschger warmings. *Nature Communications* **4**, 2849. (DOI:10.1038/ncomms3849).
[97] Thomsen, C., Blaume, F., Fohrmann, H., Peeken, I. & Zeller, U. 2001 Particle transport processes at slope environments — event driven flux across the Barents Sea continental margin. *Mar. Geol.* **175**, 237-250. (DOI:10.1016/S0025-3227(01)00143-8).
[98] Hood, E., Fellman, J., Spencer, R. G. M., Hernes, P. J., Edwards, R., D'Amore, D. & Scott, D. 2009 Glaciers as a source of ancient and labile organic matter to the marine environment. *Nature* **462**, 1044. (DOI:10.1038/nature08580).
[99] Bhatia, M. P., Das, S. B., Xu, L., Charette, M. A., Wadham, J. L. & Kujawinski, E. B. 2013 Organic carbon export from the Greenland ice sheet. *Geochimica et Cosmochimica Acta* **109**, 329-344. (DOI:10.1016/j.gca.2013.02.006).
[100] Deng, L., Bölsterli, D., Kristensen, E., Meile, C., Su, C.-C., Bernasconi, S. M., Seidenkrantz, M.-S., Glombitza, C., Lagostina, L., Han, X., et al. 2020 Macrofaunal control of microbial community structure in continental margin sediments. *Proceedings of the National Academy of Sciences* **117**, 15911-15922. (DOI:10.1073/pnas.1917494117).
[101] Faust, J. C., Stevenson, M. A., Abbott, G. D., Knies, J., Tessin, A., Mannion, I., Ford, A., Hilton, R., Peakall, J. & März, C. 2020 Does Arctic warming reduce preservation of organic matter in Barents Sea sediments? *Philosophical Transactions of the Royal Society A*.

[102] Barton, B. I., Lenn, Y.-D. & Lique, C. 2018 Observed atlantification of the Barents Sea causes the Polar Front to limit the expansion of winter sea ice. *Journal of Physical Oceanography* **48**, 1849–1866. (DOI:10.1175/JPO-D-18-0003.1).

Figure and table captions

Figures

Figure 1: Bulk organic, inorganic and grain size data against depth (cm) to highlight changes taking place below the sediment-water interface with age estimation at 27.5 cm depth for radiocarbon (^{14}C-AMS) on planktonic and benthic foraminifera. Bulk organic parameters include: total organic carbon (TOC), total nitrogen (N), TOC:N ratio and nitrogen stable isotopes (δ^{15}N). Bulk inorganic parameters include iron (Fe), phosphorus (P) and Manganese (Mn). Grain size is plotted on a % cumulative basis, categorised in six size fractions (<2 μm, 2-63 μm, 63-128 μm, 128-250 μm, 250-500 μm, 500 - 2000 μm).

Figure 2: Organic geochemical parameters plotted against depth (cm) with $^{f\text{-}SPI}L_{mean}$ (0.5 cm, average of three replicates) and $^{f\text{-}SPI}L_{max}$ (4.3 cm, greatest of three replicates) bioturbation depths indicated, together with bioturbation activity (insert provides detail 0-4.5 cm) [50]. For *n*-alkanoic acids parameters include total FAMEs (fatty acid methyl esters), ratio of the C_{15} anteiso/C_{16} FAME, terrigenous to aquatic fatty acid ratio (TAR_{FA}) [34] and total carbon preference index (CPI_T) [35]. For sterols parameters include cholesterol/brassicasaterol, cholesterol/β-sitosterol, stigmasterol/stigmastanol and β-sitosterol/stigmastanol. For *n*-alkanes parameters include carbon preference index (CPI) [36] and odd over even predominance for *n*-$C_{17\text{-}21}$ & *n*-$C_{21\text{-}25}$ ($OEP_{17\text{-}21\ \&\ 21\text{-}25}$) [37]. For *n*-alkanols parameters include terrestrial to aquatic ratio (TAR) and Aut/All (autochthonous/allochthonous) ratio [38].

Figure 3: Microbial parameters plotted against depth (cm) with mean and maximum bioturbation depths indicated, bioturbation activity (insert provides detail 0-4.5 cm) [50], coincident pore-water oxygen transition [29] and modeled relative contribution of metabolic pathway to OM heterotrophic degradation [29]. Microbial parameters include 16s RNA bacteria, 16s RNA archaea, *Nitrosopumilaceae, Shewanellaceae, Desulfuromonadales, Methylomirabilaceae,* and *Desulforbacteraceae*. Modeled data include relative aerobic respiration, denitrification, iron reduction, sulfate reduction and manganese reduction [29].

Figure 4: Principal components analysis (PCA) of bulk organic, inorganic, organic geochemical, geomicrobiological and modeled processes [29] based on $\log^{10}$ transformed and centred datasets. Samples within the uppermost oxic and bioturbated layer [50] to ~4.5 cm depth are indicated by blue circles with deeper layers indicated by red circles.

Supplements

Supplementary Table S1 – Summary of analyses and purpose for cores from B15.
Supplementary Figures S1 – S7 – Map of study location in the Barents Sea, correlations between key geochemical, modeled and measured datasets. PCA axis 1 & 2 scores plotted against depth.
Supplementary information datasets – Datasets utilised within this study.

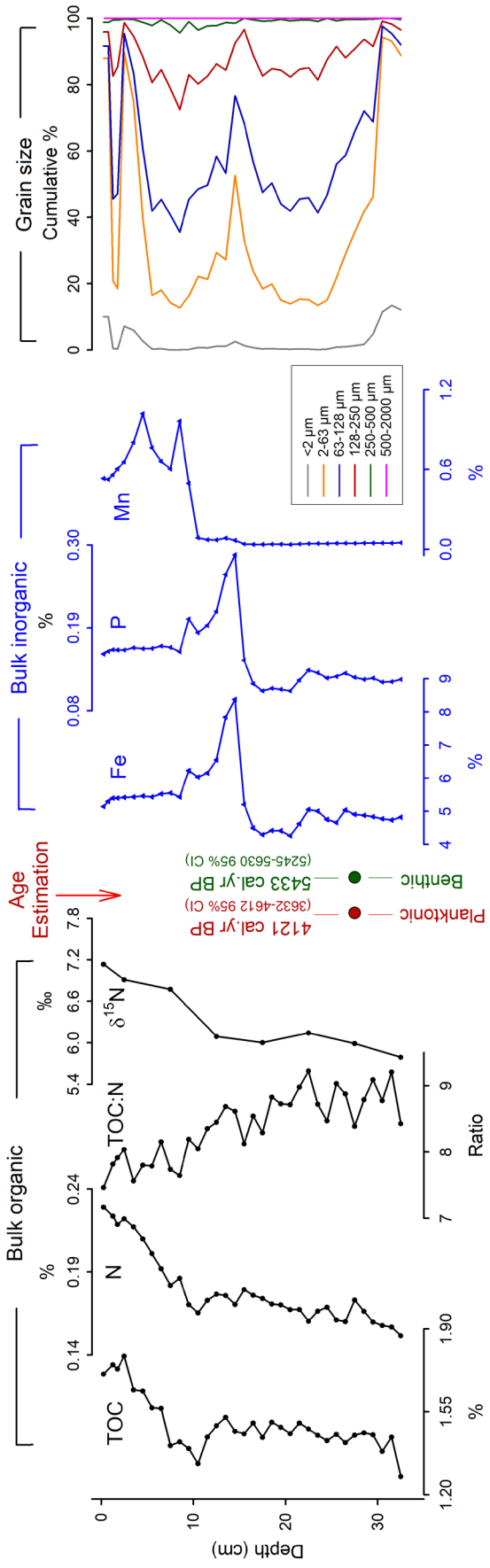
Grain size
Cumulative %
<2 µm
2-63 µm
63-128 µm
128-250 µm
250-500 µm
500-2000 µm
Bulk inorganic
%
Mn
P
Fe
Age
Estimation
Planktonic
Benthic
4121 cal.yr BP
(3632-4612 95% CI)
5433 cal.yr BP
(5245-5630 95% CI)
Bulk organic
‰
δ^{15}N
TOC:N
Ratio
N
TOC
Depth (cm)

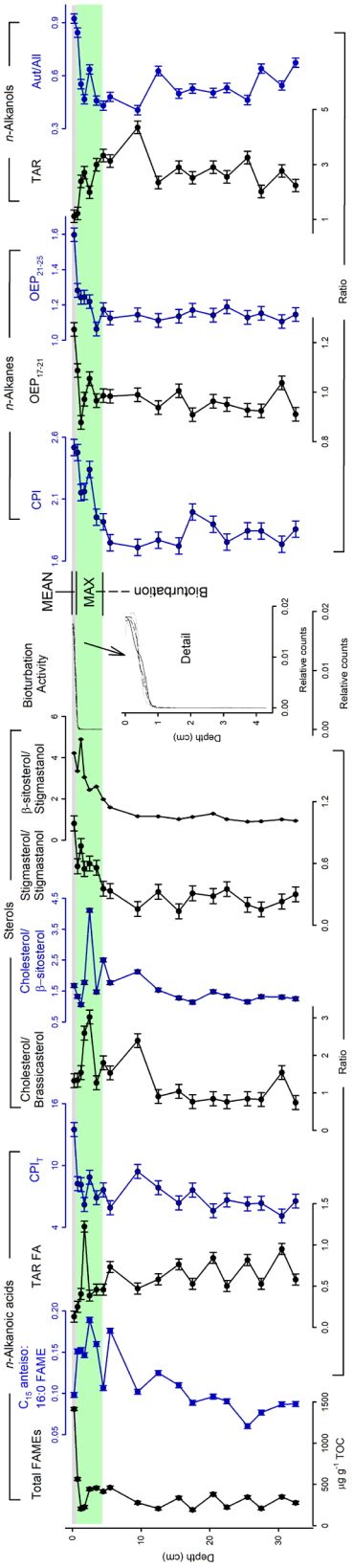
n-Alkanoic acids
Total FAMEs
C18 anteiso: 16:0 FAME
TAR FA
CPIT
Sterols
Cholesterol/ Brassicasterol
Cholesterol/ β-sitosterol
Stigmasterol/ Stigmastanol
β-sitosterol/ Stigmastanol
Bioturbation Activity
Detail
Relative counts
MEAN
MAX
Bioturbation
n-Alkanes
CPI
OEP17-21
OEP21-25
n-Alkanols
TAR
Aut/All
Ratio
µg g-1 TOC
Depth (cm)

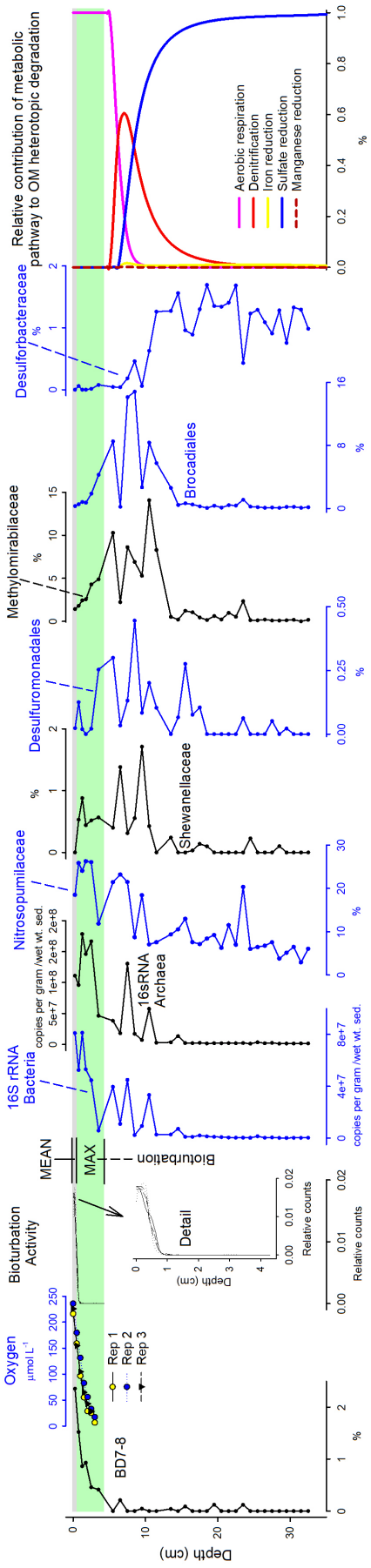
Depth (cm)
Oxygen
µmol L⁻¹
Rep 1
Rep 2
Rep 3
BD7-8
%
Bioturbation Activity
MEAN
MAX
Biotrbation
Detail
Relative counts
16S rRNA Bacteria
copies per gram /wet wt. sed.
Nitrosopumilaceae
16sRNA Archaea
Shewanellaceae
Desulfuromonadales
Methylomirabilaceae
Brocadiales
Desulforbacteraceae
Relative contribution of metabolic pathway to OM heterotopic degradation
Aerobic respiration
Denitrification
Iron reduction
Sulfate reduction
Manganese reduction

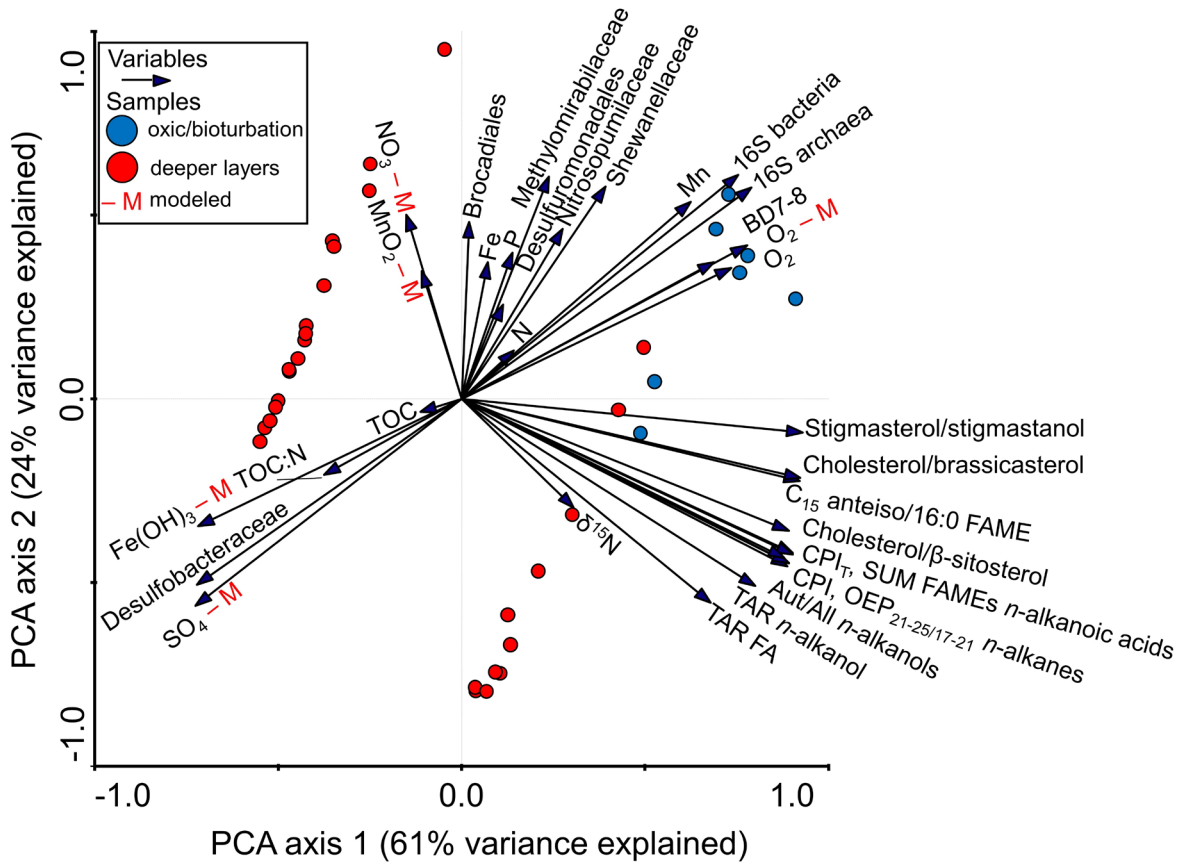
Variables
Samples
oxic/bioturbation
deeper layers
– M modeled
PCA axis 2 (24% variance explained)
PCA axis 1 (61% variance explained)
1.0
0.0
-1.0
-1.0
0.0
1.0
NO3 – M
MnO2 – M
Brocadiales
Methylomirabilaceae
Desulfuromonadales
Nitrosopumilaceae
Shewanellaceae
Fe
P
N
Mn
16S bacteria
16S archaea
BD7-8
O2 – M
O2
TOC
TOC:N
Fe(OH)3 – M
Desulfobacteraceae
SO4 – M
δ15N
Stigmasterol/stigmastanol
Cholesterol/brassicasterol
C15 anteiso/16:0 FAME
Cholesterol/β-sitosterol
CPIT, SUM FAMEs n-alkanoic acids
CPI, OEP21-25/17-21 n-alkanes
Aut/All n-alkanols
TAR n-alkanol
TAR FA